JOURNAL OF COMPUTATIONAL PHYSICS **129,** 111–120 (1996)
ARTICLE NO. 0237

Sparse Boundary Conditions on Artificial Boundaries for Three-Dimensional Potential Problems

A. S. Deakin and H. Rasmussen

Department of Applied Mathematics, University of Western Ontario, London, Ontario, Canada N6A 5B7

Received December 5, 1994; revised April 10, 1996

We consider Laplace's equation in three dimensions where the domain is restricted to a finite region with the introduction of an artificial boundary B on which a boundary condition is imposed. The finite difference method is employed to compare the solution at the nodes inside and on the surface B for four different boundary conditions of which two are local and two are nonlocal. The standard nonlocal (DtN) boundary condition is derived from the solution of the exterior Dirichlet problem, and a discretized (DDtN) version is derived that applies at the nodes on B. However, the coefficients associated with the nodes on B in the system of linear equations for the solution is not sparse. This lack of sparsity is acute for three-dimensional problems owing to the large number of equations. The DDtN boundary condition is approximated to obtain a sparse nonlocal boundary condition, where the coefficients associated with the nodes on B are relatively sparse. We show that the DDtN solution is very accurate. In addition, we present results which indicate that the difference between the DDtN solution and the solution for each of the other three boundary conditions has the correct behavior when the artificial boundary is enlarged.

1. INTRODUCTION

In considering Laplace's equation or the reduced wave equation in an infinite domain, an artificial boundary B is often introduced, along with boundary conditions on B, so that the computational domain inside B is sufficiently small for accurate numerical work.

The simplest local boundary condition to impose on B is the "condition at infinity." As shown by Keller and Givoli [1] and by Fix and Marin [2] for the reduced wave equation, the Sommerfeld radiation condition on B may introduce spurious reflection of waves from B. As a consequence, large errors may appear in the numerical solution. In the problem we consider for Laplace's equation, specifying the flux on B, which is the condition at infinity, gives inaccurate numerical solutions compared with a second local boundary condition that is generated using the approach of Bayliss *et al.* [3].

In [3] a sequence of boundary conditions on B that provide progressively more accurate numerical solutions is derived for the reduced wave equation and Laplace's equation in spherical coordinates (r, θ, ϕ). For Laplace's equation where the solution has the form $u = \sum_{j=1}^{\infty} r^{-j} F_j(\theta, \phi)$, the sequence of boundary conditions is

$$B_m u = \prod_{j=1}^{m} \left(\frac{\partial}{\partial r} + \frac{2j-1}{r} \right) u = 0, \tag{1}$$

where the artificial boundary is a sphere. $B_1 u = 0$ is the simplest case, and the second case, $B_2 u = 0$, can be expressed in the form

$$\frac{\partial u}{\partial r} = -\frac{u}{r} + \frac{\partial(\partial u/\partial\theta \sin\theta)/\partial\theta}{2r \sin\theta}, \tag{2}$$

where Laplace's equation is used to eliminate $\partial^2 u/\partial r^2$ and $u = u(r, \theta)$. Numerical results are presented for Neumann data on the sphere $r_0 = 0.5$ corresponding to a monopole or a dipole at $r = 0.2$ or $r = 0.4$. The artificial boundary is a sphere where the radius r_1 varies from 0.57 to 0.65. The error is substantially reduced using $B_2 u = 0$ rather than $B_1 u = 0$.

The nonlocal boundary condition that relates the Neumann datum at a point on B to the Dirichlet data at all the points on B is referred to as the DtN boundary condition in [1]. This boundary condition is derived by solving the Dirichlet problem in the domain exterior to B. As a consequence, only simple artificial boundaries (a circle in two dimensions or a sphere or a cylinder in three dimensions) are usually considered owing to the complexities of the boundary condition in other coordinate systems.

The numerical accuracy of the DtN boundary condition when compared with the exact solution is discussed by Keller and Givoli [1] and by Fix and Marin [2]. In [1], for the reduced wave equation in two dimensions, the exact solution is compared to the solutions obtained using the DtN boundary condition, the Sommerfeld radiation condition, and three other local boundary conditions, two of which were proposed by Engquist and Majda [4]. The DtN solution was close to the exact solution while the solutions obtained using the local boundary conditions had relatively large errors. In [2], the authors consider wave propagation

0021-9991/96 $18.00

problems in layers of the type that arise in underwater acoustics. They discuss numerical results for the reduced wave equation in a cylindrical region in which the DtN boundary condition is applied on the artificial cylindrical boundary and the acoustic potential on the inner cylinder is sin ωz for various frequencies ω. In one set of numerical experiments, the DtN solution is compared with the exact solution. As stated previously, the wall reflections that occur if the classical radiation condition is applied on B are also illustrated.

In Refs. [1, 2], the DtN boundary condition is expressed in terms of the eigenfunctions of the exterior Dirichlet problem. Alternatively, there are other forms of the DtN boundary condition. In MacCamy and Marin [5] and Marin [6], where they consider the reduced wave equation in two dimensions, the boundary condition is defined by integral equations involving the free space Green's function. Although this representation holds for noncircular curves B, it is computationally convenient to choose B as a circle. In the latter case, the representation of the DtN boundary condition in terms of a Green's function is also presented in Givoli and Keller [7]. In Deakin and Dryden [8], the DtN boundary condition is determined numerically for Laplace's equation in two dimensions by using the free space Green's function directly. By considering an appropriate distribution of point sources within B, the matrix, that relates the Neumann data to the Dirichlet data at the nodes on B, can be determined numerically.

Another approach is developed by Tam and Webb [9] for the Helmholtz equation, where the boundary condition on the artificial boundary is determined from the asymptotic expansion of the finite difference equations. The boundary conditions derived in this way are compatible with the finite difference equations in the computational zone. The numerical results are free of reflections even when the number of grid points per wavelength is as low as five.

The authors would like to thank one of the referees for mentioning the review article by Givoli [10]. This paper presents an excellent introduction to the boundary condition on artificial boundaries for the scalar as well as the reduced wave equation. Examples are provided to show that some boundary conditions introduce large spurious reflection of waves; hence, large errors appear in the computed solution. In addition, there is an extensive reference to the areas of application where non-reflecting boundary conditions on artificial boundaries are employed.

In Section 2, we formulate the boundary value problem that we consider, and we present two local boundary conditions (LBC1 and LBC2). The DtN boundary condition on a cylinder is derived in Section 3. We define nodes on this cylinder and determine the discretized DtN (DDtN) boundary condition that is used in our calculations. In Section 4, we approximate the DDtN boundary condition to obtain a sparse nonlocal boundary condition (SNBC). Our numerical approach is described in Section 5, and the accuracy of the four boundary conditions as well as other computational details are presented in Section 6.

2. FORMULATION

Consider the space between two insulated planes located at $z = 0$ and $z = 1$, where (r, θ, z) is a cylindrical polar coordinate system. Between the planes is a domain Ω^* with boundary $\partial\Omega^*$ which contains a perfectly conducting electrode held at a constant potential, that can be taken to be unity. Far from the electrode the total flux is given by F, another prescribed parameter. Thus we wish to find the potential ϕ given by

$$\nabla^2\phi = 0 \tag{3}$$

and

$$\phi = 1 \quad \text{on } \partial\Omega^* \tag{4}$$

$$\frac{\partial\phi}{\partial z} = 0 \quad \text{at } z = 0, 1 \tag{5}$$

$$\frac{\partial\phi}{\partial r} = \frac{F}{2\pi r} + O\left(\frac{1}{r^2}\right) \quad \text{as } r \to \infty. \tag{6}$$

The main difficulty is the treatment of the condition at infinity. To this end, we introduce a cylindrical artificial boundary of radius R on which we impose boundary conditions. The nonlocal boundary conditions are derived in the next two sections. We now describe the two local boundary conditions that can be imposed on the artificial boundary.

To determine local boundary conditions on $r = R$, we start with the first few terms in the eigenfunction expansion of the exterior Dirichlet problem (see (14)). For large r

$$\phi(r, \theta, z) = \frac{F}{2\pi}\ln r + C + \frac{f(\theta)}{r} + O\left(\frac{1}{r^2}\right), \tag{7}$$

where C is a constant, $f(\theta)$ is a function of θ, and F is the total flux. Upon differentiating ϕ, we have

$$\frac{\partial\phi}{\partial r} = \frac{F}{2\pi r} - \frac{f(\theta)}{r^2} + O\left(\frac{1}{r^3}\right). \tag{8}$$

Thus the first local boundary condition (LBC1) is obtained by applying the ''condition at infinity'' on the artificial boundary at $r = R$,

$$\frac{\partial\phi}{\partial r} - \frac{F}{2\pi r} = 0, \tag{9}$$

where the error in ϕ, using this boundary condition, is $O(1/r)$. To generate the second local boundary condition, we use the approach of Bayliss *et al.* [3] and apply the operator $\partial/\partial r + 2/r$ to (8) in order to eliminate the term $f(\theta)/r^2$. Hence,

$$\left(\frac{\partial}{\partial r} + \frac{2}{r}\right)\frac{\partial \phi}{\partial r} = \frac{F}{2\pi r^2} + O\left(\frac{1}{r^4}\right) \tag{10}$$

so that the second local boundary condition (LBC2) is

$$\frac{\partial^2 \phi}{\partial r^2} + \frac{2}{r}\frac{\partial \phi}{\partial r} - \frac{F}{2\pi r^2} = 0 \tag{11}$$

and the error in ϕ using this boundary condition is $O(1/r^2)$. For another form for this boundary condition, we substitute for ϕ_{rr} from Laplace's equation to obtain

$$\frac{\partial \phi}{\partial r} = \frac{F}{2\pi r} + \frac{1}{r}\frac{\partial^2 \phi}{\partial \theta^2} + r\frac{\partial^2 \phi}{\partial z^2}. \tag{12}$$

Let us now consider the treatment of the boundary condition (4) on the surface of the charged electrode. It is relatively easy to model this condition for a given electrode of a regular shape, such as a circular cylinder. However, for irregular shapes it is tedious to change the program for each change of electrode shape. We avoid this problem by using the expression $\phi = 1$ as the governing equation inside and on the boundary of the electrode. If there are N nodes in the finite difference scheme inside and on the boundary, then we add N additional equations $\phi = 1$ to the set of difference equations derived from Laplace's equation. The sparse matrix solver will easily find the solution $\phi = 1$ at the nodes inside and on the boundary so that the boundary condition is satisfied. Let Ω be the domain interior to the cylinder $r = R$ and exterior to the electrode while Ω^* is the domain occupied by the electrode. Thus we will solve (3) in Ω, together with the boundary conditions at $z = 0, 1$ and $r = R$, and we replace (4) by

$$\phi = 1 \quad \text{in } \Omega^*. \tag{13}$$

3. THE DtN BOUNDARY CONDITION

We derive the exact nonlocal boundary condition on the cylinder of radius R that relates $\partial\phi/\partial r$ at one point on the cylinder with ϕ at all the points. Then nodes are defined on the cylinder so that the boundary condition relates $\partial\phi/\partial r$ at one node to ϕ at all the nodes.

The exact solution of the exterior Dirichlet problem can be readily obtained in the form

$$\phi(r, \theta, z) = \frac{F}{2\pi}\ln\frac{r}{R} + \sum_{n=0}^{\infty}\sum_{m=0}^{\infty}\frac{G_{mn}(r)}{G_{mn}(R)} \cos(m\pi z)(C_{mn}\cos n\theta + D_{mn}\sin n\theta) \quad (r \geq R), \tag{14}$$

where

$$G_{mn}(r) = \begin{cases} r^{-n} & \text{if } m = 0 \\ K_n(m\pi r) & \text{if } m \neq 0 \end{cases} \tag{15}$$

and $K_n(m\pi r)$ is the modified Bessel function of the second kind. Assuming for the moment that ϕ is known on the cylinder of radius R, then C_{mn} and D_{mn} are the usual Fourier coefficients. From this solution, the derivative $\partial\phi/\partial r$ on the artificial boundary is

$$\frac{\partial \phi}{\partial r}(R, \theta, z) = \frac{F}{2\pi R} - \int_0^1\int_{-\pi}^{\pi} \phi(R, \theta', z')m(\theta - \theta', z, z')\, d\theta'\, dz', \tag{16}$$

where F is the total flux passing through the cylinder of radius R, and

$$m(\Theta, z, z') = \sum_{n=0}^{\infty}\cos n\Theta\left(\frac{n}{\pi R} - \sum_{m=1}^{\infty}\frac{2mK_n'(n\pi R)}{(1 + \delta_{n0})K_n(m\pi R)}\cos m\pi z \cos m\pi z'\right). \tag{17}$$

The operator in (16) that relates the Dirichlet datum ϕ to the Neumann datum $\partial\phi/\partial r$ is called the Dirichlet to Neumann (DtN) map (see [1]) and we refer to (16) as the DtN boundary condition.

For numerical work, we define nodes at (R, θ_j, z_k), where

$$\theta_j = (j - 1)2\pi/n_\theta, \quad z_k = (k - 1/2)/n_z, \quad j = 1, ..., n_\theta, \quad k = 1, ..., n_z.$$

Then we approximate $\phi(R, \theta, z)$ in terms of its values at the nodes,

$$\phi(R, \theta, z) \approx \sum_{p,q} v_{pq}(R, \theta, z)\phi(R, \theta_p, z_q), \tag{18}$$

using a basis v_{pq}, where v_{pq} is equal to 1 at the node (R, θ_p, z_q) and zero at all other nodes. Substituting this expression for ϕ into (16), we have an expression for the boundary condition of the form

$$\frac{\partial \phi}{\partial r}(R, \theta_j, z_k) = \frac{F}{2\pi R} - \sum_{p=1}^{n_\theta} \sum_{q=1}^{n_z} M_{j,k}^{p,q} \phi(R, \theta_p, z_q), \quad (19)$$

where

$$M_{j,k}^{p,q} = \int_0^1 \int_{-\pi}^{\pi} v_{pq}(R, \theta', z') m(\theta_j - \theta', z_k, z')\, d\theta'\, dz'. \quad (20)$$

We could use the finite element method in which v_{pq} are defined in terms of shape functions (see [1]). In this approach, the integrals in (20) are evaluated numerically. However, in our case, where the eigenfunctions are not complicated, we define v_{pq} in terms of a subset of the eigenfunctions in (14) for the exterior Dirichlet problem. That is, we construct the solution $\phi_D(r, \theta, z)$ that approximates $\phi(r, \theta, z)$ in the domain exterior to the cylinder $r = R$ such that ϕ_D is equal to ϕ at the nodes on the cylinder. Let

$$\phi_D(r, \theta, z) = \frac{F}{2\pi} \ln \frac{r}{R} + \sum_{p,q} v_{pq}(r, \theta, z) \phi(R, \theta_p, z_q), r \geq R, \quad (21)$$

where

$$v_{pq}(r, \theta, z) = \sum_{n=0}^{n_\theta/2} \sum_{m=0}^{n_z-1} \frac{G_{mn}(r)}{G_{mn}(R)} \cos(m\pi z)(A_{mn}^{pq} \cos n\theta + B_{mn}^{pq} \sin n\theta), \quad (22)$$

and the $n_\theta \times n_z$ coefficients A_{mn}^{pq} and B_{mn}^{pq} ($B_{mn}^{pq} = 0$ for $n = n_\theta/2$) are uniquely determined from the $n_\theta \times n_z$ conditions

$$v_{pq}(R, \theta_j, z_k) = \delta_{pj}\delta_{qk}. \quad (23)$$

Once $v_{pq}(r, \theta, z)$ is known, $M_{j,k}^{p,q}$ can be readily simplified using the orthogonality properties of the eigenfunctions for the exterior Dirichlet problem. Note that the only approximation in the boundary condition (19) is the approximation (18) of ϕ in terms of the finite basis; hence, we refer to (19) as the discretized DtN (DDtN) boundary condition.

In the determination of the coefficients in (22), we require the orthogonality properties,

$$\sum_{j=1}^{n_\theta} \cos n\theta_j \cos n'\theta_j = \varepsilon_{nn'} n_\theta/2 \ (n, n' = 0, ..., n_\theta/2) \quad (24)$$

$$\sum_{j=1}^{n_\theta} \sin n\theta_j \sin n'\theta_j = (2\delta_{nn'} - \varepsilon_{nn'}) n_\theta/2 \quad (25)$$

$$\sum_{j=1}^{n_\theta} \sin n\theta_j \cos n'\theta_j = 0 \quad (26)$$

$$\sum_{k=1}^{n_z} \cos(m\pi z_k)\cos(m'\pi z_k) = \begin{cases} n_z & \text{if } m = m' = 0 \\ \delta_{mm'} n_z/2 & \text{if } 0 < m + m' < 2n_z, \end{cases} \quad (27)$$

where

$$\varepsilon_{nn'} = \begin{cases} \delta_{nn'} & \text{if } n \neq 0, n \neq n_\theta/2 \\ 2\delta_{nn'} & \text{if } n = 0 \text{ or } n = n_\theta/2 \end{cases} \quad (28)$$

and $\delta_{nn'}$ is the Kronecker delta. Using these orthogonality properties, the coefficients for v_{pq} in (22) are given by

$$(1 + \delta_{m0}) A_{mn}^{pq} \varepsilon_{nn} n_\theta n_z/4 = \cos n\theta_p \cos m\pi z_q \quad (29)$$

$$(1 + \delta_{m0}) B_{mn}^{pq} \varepsilon_{nn} n_\theta n_z/4 = \sin n\theta_p \cos m\pi z_q. \quad (30)$$

Upon substituting (29) and (30) into (22), we have

$$v_{pq}(r, \theta, z) = \sum_{n=0}^{n_\theta/2} \sum_{m=0}^{n_z-1} \frac{4G_{mn}(r)}{G_{mn}(R)\varepsilon_{nn}(1 + \delta_{m0}) n_\theta n_z} \cos m\pi z \cos m\pi z_q \cos n(\theta - \theta_p). \quad (31)$$

$M_{j,k}^{p,q}$ can now readily be expressed in a simpler form by substituting (31) into (20) and using the orthogonality properties of the eigenfunctions for the exterior Dirichlet problem. The result is

$$M_{j,k}^{p,q} = \sum_{n=0}^{n_\theta/2} \sum_{m=0}^{n_z-1} A_{mn} \cos n(\theta_p - \theta_j) \cos m\pi z_k \cos m\pi z_q, \quad (32)$$

where

$$A_{mn} = \begin{cases} 2n/(R\varepsilon_{nn} n_\theta n_z) & \text{if } m = 0 \\ \dfrac{-4m\pi K_n'(m\pi R)}{K_n(m\pi R)\varepsilon_{nn} n_\theta n_z} & \text{if } m \neq 0. \end{cases} \quad (33)$$

The following mathematical properties are important and provide an interpretation of (19) and (32):

(a) $M_{j,k}^{p,q}$ in (32) is equal to $-\partial v_{pq}/\partial r$ evaluated at the (R, θ_j, z_k) node; and, thus, $M_{j,k}^{p,q}$ is the flux at the node for the solutions v_{pq} that form the basis for ϕ on the boundary. To prove this property, substitute (21) into (19).

(b) Since $\sum_{j,k} M_{j,k}^{p,q} = 0$, which follows directly from (32) using the orthogonality properties (24) to (27), then $F/(2\pi R)$ in (19) is the average value of $\partial\phi/\partial r$ at the nodes.

(c) First, the solution ϕ_D in (21), where v_{pq} is given by (31), is the exact solution of the DDtN boundary condition

(19), and this property can be proved directly using the orthogonality conditions (24) to (27); it also follows from (16) to (20) since ϕ_D is a solution of Laplace's equation. Second, we compare the solution ϕ_D with the exact solution (14). Assuming that ϕ is known on $r = R$, the Fourier coefficients C_{mn} and D_{mn} in (14) are approximated by their Riemann sums involving ϕ at the nodes (R, θ_p, z_q). Then the coefficients in (22) are related to those in (14) as follows: $\sum_{p,q} A_{mn}^{pq}\phi(R, \theta_p, z_q) \approx C_{mn}$ and $\sum_{p,q} B_{mn}^{pq}\phi(R, \theta_p, z_q) \approx D_{mn}$ for $n < n_\theta/2$; $\sum_{p,q} A_{mn}^{pq}\phi(R, \theta_p, z_q) \approx C_{mn}/2$ for $n = n_\theta/2$. So far, we have (details below)

$$\phi(R, \theta, z) \approx \phi_D(R, \theta, z) + \sum_{m=0}^{1} O(|C_{mn}| + |D_{mn}|)\ (n = n_\theta/2). \tag{34}$$

Third, we assume that ϕ is known on the cylinder with the smallest radius r^* that encloses Ω^* in (13). Then the solution for $r \geq r^*$ has the form (14), where

$$\phi(r, \theta, z) = \frac{F}{2\pi}\ln\frac{r}{R} + \sum_{n=0}^{\infty}\sum_{m=0}^{\infty}\frac{G_{mn}(r)}{G_{mn}(r^*)} \cos(m\pi z)(C_{mn}^* \cos n\theta + D_{mn}^* \sin n\theta). \tag{35}$$

In (14) and (35), $(C_{mn}, D_{mn}) = (C_{mn}^*, D_{mn}^*)G_{mn}(R)/G_{mn}(r^*)$ and, for $m \geq 1$, $G_{mn}(r) = O(r^{-1/2}e^{-m\pi r})$. With these details, the form of the remainder in (34) can be verified, and we have

$$\phi(R, \theta, z) \approx \phi_D(R, \theta, z) + O(\alpha_0(n_\theta/2)R^{-n_\theta/2}) + O(\alpha_1(n_\theta/2)R^{-1/2}\exp(-\pi R)), \tag{36}$$

where $|C_{mn}^*| + |D_{mn}^*| = O(\alpha_m(n))$ for n large.

(d) From a computational point of view, the symmetries of $M_{j,k}^{p,q}$ can be used to reduce the computational work required to evaluate these coefficients. These symmetries are

$$M_{j,k}^{p,q} = M_{p,q}^{j,k} = M_{j,q}^{p,k} = M_{1,k}^{|p-j|+1,q}. \tag{37}$$

Although there are $(n_\theta n_z)^2$ coefficients $M_{j,k}^{p,q}$, the number of coefficients to be computed is $(n_\theta + 2)(n_z + 1)n_z/4$ owing to these symmetries.

4. SPARSE NONLOCAL BOUNDARY CONDITION

While the above approach leads to a very accurate boundary condition (19), it does have the drawback of producing a fairly dense set of linear equations for the values of $\phi(R, \theta_j, z_k)$. This means that the sparse matrix solver, described in Section 5, is not so efficient and requires considerably more memory on the workstation. After some experimentation, we found an approximation of the boundary condition (19) for which the sparsity of the system of equations is improved; moreover, the numerical solution is accurate. We refer to this sparse nonlocal boundary condition as SNBC. We start with our principal result.

The DDtN boundary condition (19) *can be approximated as*

$$\frac{\partial\phi}{\partial r}(R, \theta_j, z_k) = \frac{F}{2\pi R} - \sum_{p,q} L_{j,k}^{p,q}\phi(R, \theta_p, z_q), \tag{38}$$

where

$$L_{j,k}^{p,q} = P_k^q\delta_{pj} + Q_j^p\delta_{qk} \tag{39}$$

$$P_k^q = \sum_p M_{j,k}^{p,q}, \quad Q_j^p = \sum_q M_{j,k}^{p,q}. \tag{40}$$

$L_{j,q}^{p,q}$ has $n_z + n_\theta/2$ nonzero coefficients which occur at the nodes (R, θ_p, z_k), that lie on a circle, and at the nodes (R, θ_j, z_q), that lie on a straight line, where the circle and the line on the cylinder pass through the node (R, θ_j, z_k).

In effect, the coefficients in (38) are readily obtained by lumping together the coefficients in (19) at a few nodes in the following manner. The coefficient $L_{j,k}^{p,k}$ at (R, θ_p, z_k) $(p \neq j)$ is obtained by summing the coefficients of $M_{j,k}^{p,q}$ at the nodes on the line through (R, θ_p, z_k). Similarly, the coefficient $L_{j,k}^{j,q}$ at (R, θ_j, z_q) $(q \neq k)$ are obtained by summing $M_{j,k}^{p,q}$ at the nodes on the circle through (R, θ_j, z_q). At (R, θ_j, z_k), $L_{j,k}^{j,k}$ is equal to the sum of $M_{j,k}^{p,q}$ over the nodes on the line plus the sum of $M_{j,k}^{p,q}$ over the nodes on the circle, where the line and the circle pass through (R, θ_j, z_k). We now present two sets of properties of our SNBC.

First, both boundary conditions (19) and (38) are the same if the solution is independent of θ or z. In these two cases, we have, respectively,

$$\frac{\partial\phi}{\partial r}(R, z_k) = \frac{F}{2\pi R} - \sum_q P_k^q\phi(R, z_q), \qquad \frac{\partial\phi}{\partial r}(R, \theta_j) = \frac{F}{2\pi R} - \sum_p Q_j^p\phi(R, \theta_p) \tag{41}$$

since $\sum_p Q_j^p = 0$ and $\sum_q P_k^q = 0$ from properties (a) and (d) in Section 3. The former is the DDtN boundary condition for problems with axial symmetry; whereas, the latter is the DDtN boundary condition for Laplace's equation in two dimensions. The coefficients P_k^q and Q_j^p can be expressed in closed form using (32) and the orthogonality properties (24) to (27). For Q_j^p, we have

$$Q_j^p = \sum_q M_{j,k}^{p,q} = \frac{1}{R}$$

$$\begin{cases} [(-1)^\sigma - 1][2n_\theta \sin^2(\sigma\pi/n_\theta)]^{-1} & \text{if } \sigma = |p-j| \neq 0 \\ n_\theta/4 & \text{if } p = j. \end{cases} \tag{42}$$

Note that half of these coefficients are zero so that $L_{j,k}^{p,q}$ has $n_z + n_\theta/2$ nonzero coefficients.

Second, to describe the difference between the boundary conditions (19) and (38), we consider

$$\sum_{p,q} (M_{j,k}^{p,q} - L_{j,k}^{p,q}) \phi(R, \theta_p, z_q) = E_{j,k} \tag{43}$$

and show that $E_{j,k}$ decays exponentially for large R. Suppose, as in (c) in the last section, that ϕ is known on $r = r^*$ then ϕ is given by (35). Substituting (35) for ϕ into (43) and, noting that the sum of $M_{j,k}^{p,q} - L_{j,k}^{p,q}$ in p or q is zero, we have

$$E_{j,k} = \sum_{p,q} \sum_{n,m=1}^{\infty} (M_{j,k}^{p,q} - L_{j,k}^{p,q}) \frac{K_n(m\pi R)}{K_n(m\pi r^*)} \cos m\pi z_q (C_{mn}^* \cos n\theta_p + D_{mn}^* \sin n\theta_p). \tag{44}$$

The next step is to show that

$$M_{j,k}^{p,q} - L_{j,k}^{p,q} = O(R^{-1}) \tag{45}$$

for large R. This result is proved using the asymptotic expansion for the modified Bessel functions and the dual orthogonality identity

$$\sum_{n=0}^{n_\theta/2} \varepsilon_{nn}^{-1} \cos n(\theta_j - \theta_p) = \delta_{pj} n_\theta/2 \tag{46}$$

that follows from (31), where $r = R$, $\theta = \theta_j$ and $z = z_k$. Hence, from (44), we have

$$E_{j,k} = O(R^{-3/2} e^{-\pi R}). \tag{47}$$

We now estimate the difference between the DDtN solution ϕ_D defined by (21), which is a solution of (19), and the SNBC solution ϕ_S which satisfies (38). Only those terms in ϕ that involve both θ and z appear in (44), and the asymptotic estimate in (47) is due to the $m = 1$ terms of the form $K_n(\pi R)\cos \pi z_q$. We conjecture that $\phi_S(R, \theta_j, z_k)$ has the form

$$\phi_S(R, \theta_j, z_k) = \phi_D(R, \theta_j, z_k) + R_{j,k}(1 + O(R^{-2})) + O(R^{-1/2} e^{-2\pi R}), \tag{48}$$

where

$$R_{j,k} = -\sum_{n=1}^{n_\theta/2} K_n(\pi R)\cos(\pi z_k)(C_{1n}^* \cos n\theta_j + D_{1n}^* \sin n\theta_j)/\mathrm{K}_n(\pi r^*). \tag{49}$$

To support this conjecture, we substitute (48) into (38) and simplify the equation using the identities ($m \neq 0$)

$$\sum_q P_k^q \cos(m\pi z_q) = -m\pi \frac{K_0'(m\pi R)}{K_0(m\pi R)} \cos(m\pi z_k),$$
$$\sum_p Q_j^p \begin{Bmatrix} \cos n\theta_p \\ \sin n\theta_p \end{Bmatrix} = \frac{n}{R} \begin{Bmatrix} \cos n\theta_j \\ \sin n\theta_j \end{Bmatrix} \tag{50}$$

$$K_0'(m\pi R)/K_0(m\pi R) = K_n'(m\pi R)/K_n(m\pi R) + O(R^{-2}). \tag{51}$$

The identities in (50) are derived from (32) and (40), along with the orthogonality properties (24) to (27). In conclusion, the difference between the DDtN and SNBC solutions for large R is

$$\phi_S(R, \theta_j, z_k) - \phi_D(R, \theta_j, z_k) = O(R^{-1/2} e^{-\pi R}). \tag{52}$$

5. NUMERICAL PROCEDURE

The numerical procedure consists of replacing the potential equation in Ω by a system of finite difference equations and using (13) in Ω^*. Since this system is very sparse, we will use a sparse matrix procedure for solving it.

We use a uniform finite difference grid with nodes at (r_i, θ_j, z_k) and define

$$\phi_{i,j,k} = \phi(i\Delta r, (j-1)\Delta\theta, (k - \tfrac{1}{2})\Delta z) = \phi(r_i, \theta_j, z_k), \tag{53}$$

where $i = 1, ..., n_r + 1$, $j = 1, ..., n_\theta$, $k = 0, ..., n_z + 1$, and

$$\Delta r = \frac{R}{n_r}, \quad \Delta\theta = \frac{2\pi}{n_\theta}, \quad \Delta z = \frac{1}{n_z}. \tag{54}$$

Note that the nodes at $(r_{n_r+1}, \theta_j, z_k)$, (r_i, θ_j, z_0), and $(r_i, \theta_j, z_{n_z+1})$ are outside Ω; ϕ at these nodes appear in the finite difference equations, and the boundary conditions are used to determine an expression involving ϕ at these nodes. Finally, for the axis $r = 0$ we define

$$\phi_{0,k} = \phi(0, \theta, (k - \tfrac{1}{2})\Delta z). \tag{55}$$

For an interior point (r_i, θ_j, z_k) in Ω, or a point on the cylinder $r = R$, the derivation of the difference equation

is simple and results in

$$2(1 + D_1 + D_2)\phi_{i,j,k} - \left(1 + \frac{1}{2i}\right)\phi_{i+1,j,k} - \left(1 - \frac{1}{2i}\right)\phi_{i-1,j,k} - D_1\phi_{i,j+1,k} - D_1\phi_{i,j-1,k} - D_2\phi_{i,j,k+1} - D_2\phi_{i,j,k-1} = 0, \tag{56}$$

where

$$D_1 = \frac{1}{(i\Delta\theta)^2}, \quad D_2 = \left(\frac{\Delta r}{\Delta z}\right)^2. \tag{57}$$

This difference equation does not hold at $r = 0$, and along this line we use the mean value property of Laplace's equation and write

$$\frac{4}{(\Delta r)^2}(\phi_m - \phi) + \phi_{zz} = 0, \tag{58}$$

where ϕ_m is the mean value of ϕ at $r = \Delta r$. Thus along $r = 0$ we have the difference equation

$$(4 + 2D_2)\phi_{0,k} - \frac{4}{n_\theta}(\phi_{1,1,k} + ... + \phi_{1,n_\theta,k}) - D_2\phi_{0,k+1} - D_2\phi_{0,k-1} = 0. \tag{59}$$

In Ω^* we use the equation $\phi_{i,j,k} = 1$ for $r \neq 0$ and $\phi_{0,k} = 1$ for $r = 0$.

Consider now the boundary condition $\phi_z = 0$ at $z = 0$. When we use the difference equation (56) at $k = 1$, it will contain the term $-D_2\phi_{i,j,0}$. Now ϕ_z can be approximated by a central difference formula and the boundary condition implies that $\phi_{i,j,0} = \phi_{i,j,1}$; thus, we can replace the term $-D_2\phi_{i,j,0}$ by $-D_2\phi_{i,j,1}$. A similar treatment is applied to the boundary condition $\phi_z = 0$ at $z = 1$. The boundary condition on $r = R$ is treated in the standard way by using fictitious points at $r = R + \Delta r$.

For the solution of the sparse matrix system we used the *preconditioned biconjugate gradient stabilized method* as outlined in Barret *et al.* [11]. We used the point Jacobi preconditioner which is the simplest preconditioner; it is clear that we could have reduced the required number of iterations if we had applied a more sophisticated preconditioner such as an incomplete factorization preconditioner but this was not the object of the present investigation. We supposed that convergence was obtained when the relative updates to the solution and the residual reduction were both less than 1.0×10^{-6}. Most of the calculations were carried out in single precision, but in order to check the accuracy some were also done in double precision. Since this resulted in differences of magnitude less than 1.0×10^{-6} we decided that single precision was adequate.

The elements in the sparse matrix solver are stored in the row pointer/column used in the Yale sparse matrix package. It is generally known as the *ia*, *ja* format and requires two pointer arrays: *ia*—the array of row pointers into *ja*; and *ja*—the array of column indices. The column indices of each row are stored in the *ja* array so there is one *ja* entry for each nonzero element in the matrix. The *ia* array is a pointer to the first entry of each row. The nonzero elements of the matrix are stored in the array *a* which has the same structure as *ja*.

6. VALIDATION AND RESULTS

In this section we present some results and figures which validate the numerical procedure described in the previous section. The validation of the numerical procedure consists of three steps. In the first step we compare the approximate solution obtained using the DDtN boundary condition for a case where an analytic solution is known; we can then also estimate the rate of convergence of the procedure. An estimate of the size of the computational region which is required for an accurate solution is the second step, i.e., how small can we make R and still get an accurate solution. Since we have four different boundary conditions at $r = R$ we compare, as the third step, the accuracy obtained for a given value of R.

Let us consider the case where we have a cylinder of radius r^* with a potential ϕ^* given on the surface of this cylinder where

$$\phi^* = \cos m\pi z \cos n\theta. \tag{60}$$

Then the exact solution from (35) is

$$\phi^* = \frac{K_n(m\pi r)}{K_n(m\pi r^*)}\cos m\pi z \cos n\theta \quad (m > 0, n \geq 0). \tag{61}$$

We use this solution with $m = 2$ and $n = 4$ to test the accuracy and order of our numerical scheme.

By expanding the terms in the difference equations (56) in a Taylor series about the point (r_i, θ_j, z_k) we can show formally that the principal part T of the truncation error of our numerical scheme is

$$T = -\frac{1}{6}(\Delta r)^2\left(\frac{1}{r}\phi_{rrr} + \frac{1}{2}\phi_{rrrr}\right) + \frac{1}{12}(\Delta\theta)^2\phi_{\theta\theta\theta\theta} + \frac{1}{12}(\Delta z)^2\phi_{zzzz}, \tag{62}$$

where the higher derivatives of ϕ are evaluated at some intermediate point. Using some numerical results we show

TABLE I

Effects of Varying R

Values of R	Max difference
0.75 − 2.0	3×10^{-4}
1.00 − 2.0	3×10^{-4}
1.50 − 2.0	2×10^{-4}

that our numerical scheme is close to being second order. Let us define the maximum error E by

$$E = \max_{i,j,k} |\phi_{i,j,k} - \phi^*_{i,j,k}|. \tag{63}$$

If we consider the Δr dependence, we write the maximum error E between the exact solution and the DDtN solution in the form

$$E = A(\Delta r)^p + B, \tag{64}$$

where A and B do not depend on Δr and p is a parameter, which we will show, is very close to 2. We now calculate E for three different values of Δr with $r^* = 0.5$, $R = 1.0$, $n_\theta = 60$, and $n_z = 21$ and solve the resulting equations for A, B, and p. We find that $p = 1.93$. Similar calculations were also done for $\Delta\theta$ ($p = 2.06$) and Δz ($p = 2.16$). From this we see that our procedure is very close to being second order. The slightly lower value of p for the r dependence is undoubtedly due to the fact that the $\partial\phi/\partial r$ is not continuous at $r = r^*$. The calculated values of E also show that for this problem we must take $\Delta r \leq \frac{1}{40}$ in order for E to be less than 3.0×10^{-3}. This error E is less sensitive to reductions in $\Delta\theta$ or Δz by a factor of 2.

In order to discuss the question of the value of R which is required we apply the procedure with the DDtN boundary condition to the problem where the electrode is given by

$$0 \leq r \leq r^*, \quad \theta^* \leq \theta \leq \pi/2 + \theta^*, \quad z_1 \leq z \leq z_2, \tag{65}$$

where r^*, θ^*, z_1, z_2 are given values. For the results discussed below we used $r^* = 0.5$, $\theta^* = \pi/2$, $z_1 = 0.375$, and $z_2 = 0.875$. This is a much more difficult problem from a numerical point of view since the electrode is no longer smooth and the exact solution has singularities at these sharp edges. We decided to use the same grid spacing as before, i.e., $\Delta r = 1/40$, $\Delta\theta = 2\pi/60$, and $\Delta z = 1/21$. The results we obtain for the previous problem imply that, away from the sharp edges of the electrode, the numerical solution has an accuracy of 3.0×10^{-3}.

The question is now how close to the electrode we can place the cylinder on which we impose the DDtN boundary condition, and in Table I we show the maximum difference between solutions obtained using R equal to 0.75 and 2.0. It is interesting to note that even at $R = 0.75$ the DDtN solution is within 3×10^{-4} of that obtained for $R = 2.0$. This is remarkable since the electrode extends to $r = 0.5$ for some values of θ. Since the DDtN solution has such small changes with R, the accuracy 3.0×10^{-3} for our numerical solution, mentioned in the last paragraph, is

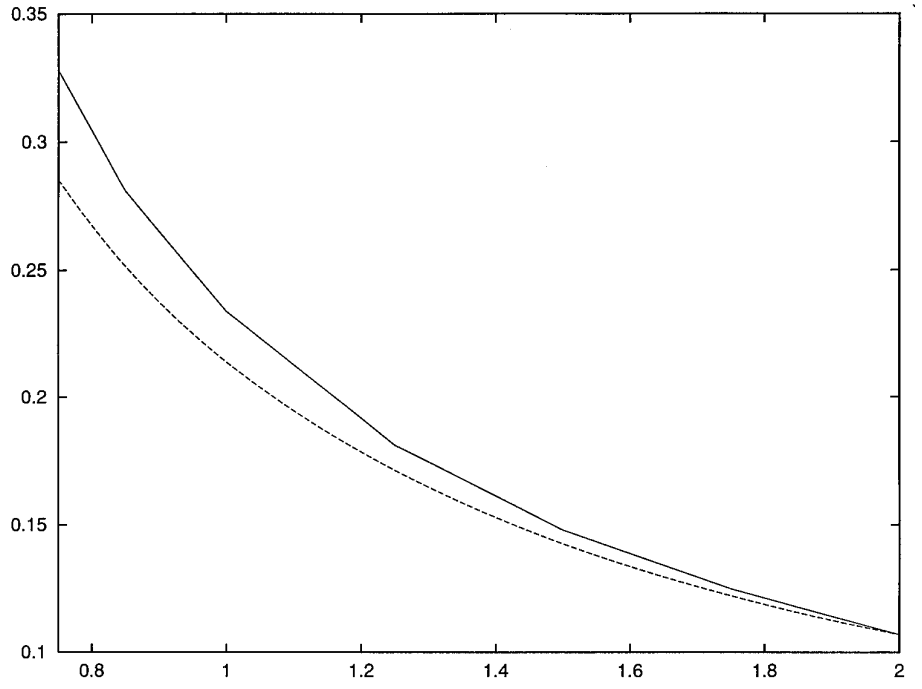

FIG. 6.1. Plot of the maximum error for the LBC1 solution vs R (solid curve) and a plot of AR^{-1} vs R, where A is a constant.

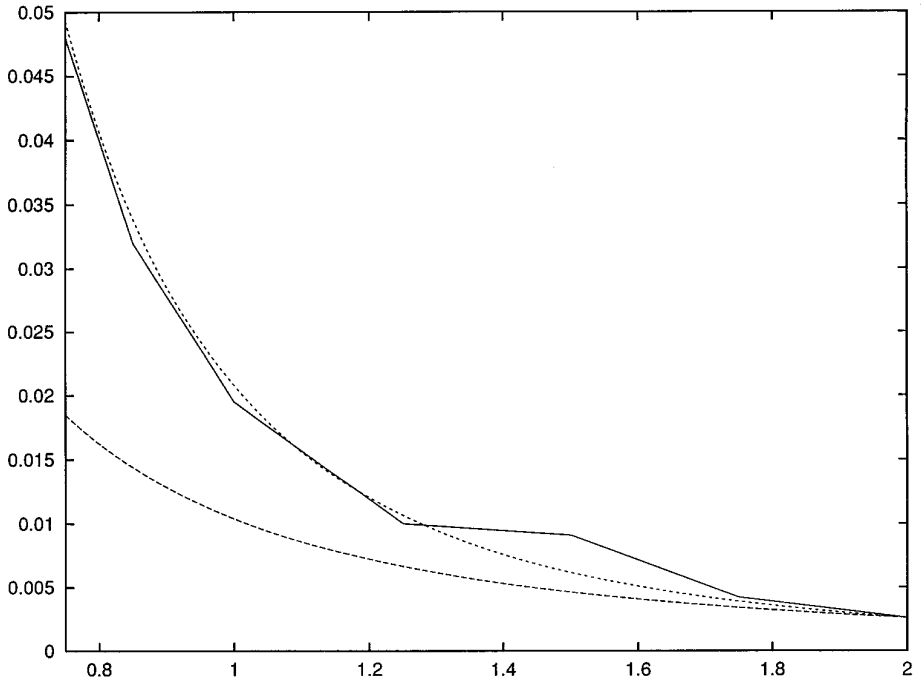

FIG. 6.2. Plot of the maximum error for the LBC2 solution vs R (solid curve) and a plot of AR^{-2} (lowest curve) and BR^{-3}, where A and B are constants.

largely truncation error. For the same reason, the verification of the estimates in (36) would require much larger computational resources.

The next point to be considered is a comparison of the accuracies that can be expected from using the four different boundary conditions. We shall assume that the DDtN solution for $R = 2.0$ is ''accurate'' and compare the other solutions to it. In Fig. 6.1 we have plotted the maximum error E, as defined above, between the DDtN solution for $R = 2.0$ and the LBC1 solution for different values of R. Since we expect that the LBC1 solution should decrease asymptotically as R^{-1} we have also plotted AR^{-1} with the constant A adjusted so that the two curves coincide at $R = 2.0$. It is clear from the graph that the error definitely decreases as R^{-1}, even for fairly small values of R. Note that the difference between the DDtN and the LBC1 solution at $R = 2.0$ is approximately equal to 0.11.

When we use LBC2, we should expect an asymptotic error of R^{-2} and Fig. 6.2 shows that this expectation is correct; however, for this case, the accuracy appears to be better than expected with an error of order R^{-3}. At $R = 2.0$, the difference between the DDtN and the LBC2 solution is approximately equal to 3.0×10^{-3}. The LBC2 solution is clearly much more accurate than the LBC1 solution. As described in Section 4 (see (52)), the difference between the DDtN and the SNBC solution should decrease as $\exp(-\pi R)R^{-0.5}$ and Fig. 6.3 shows this behaviour. At $R = 0.85$ the difference is less than 3.0×10^{-3} and it rapidly decreases to about 2×10^{-4} at $R = 1.25$. The difference is approximately 1×10^{-4} at $R = 2.0$. For $R > 1.25$, the maximum difference appears to decrease slowly, as in Table I, and this suggests that these small errors may indicate that other error estimates should be considered.

We summarize these results as follows. For $1.5 \leq R/r^* \leq 2.4$, we can only obtain a solution of accuracy of 3.0×10^{-3} if we use the DDtN boundary condition. For $R/r^* \geq 2.4$, we can use the SNBC solution. For $R/r^* = 4.0$, the error in the LBC2 and LBC1 solution could be as high as 6.0×10^{-3} and 0.11, respectively. The accuracy of the SNBC solution at $R = 0.85$ is approximately the same as the LBC2 solution at $R = 2.0$.

The last point is the increase in efficiency obtained by using a simpler form of the boundary condition at $r = R$. We have shown above that the SNBC solution for $R \geq 1.0$ is acceptable in the sense that the maximum difference

TABLE II

Timing Results

Method	Cal of matrix	Execution time	No. of matrix elements
DDtN	59 s	281 s	1,887,879
SNBC	60 s	92 s	401,079
LBC2	$\ll$1 s	110 s	306,459
LBC1	$\ll$1 s	95 s	306,459

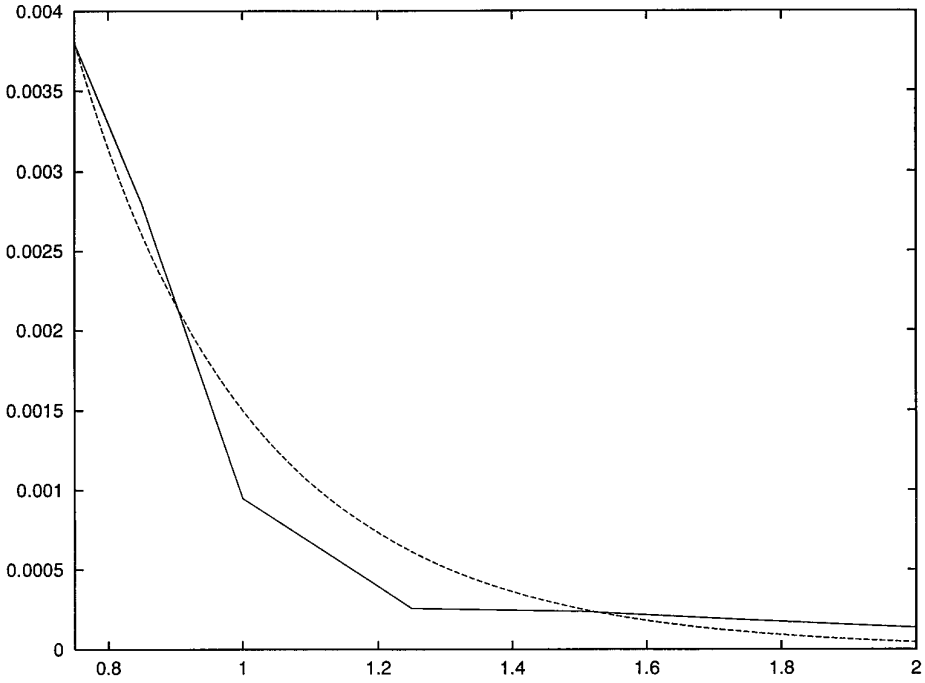

FIG. 6.3. Plot of the maximum error for the SNBC solution vs R (solid curve) and a plot of $A \exp(-\pi R)R^{-1/2}$ vs R, where A is a constant.

between the SNBC and the DDtN solutions is 0.001. It is of interest to look at the relative computing times for these two procedures since the second one definitely leads to a decrease in the number of nonzero coefficients in the system of linear equations.

The number of nonzero coefficients from the discretization of Laplace's equation is approximately $7(n_r - 1)n_\theta n_z$ and the additional number generated from the DDtN boundary condition at $r = R$ is $(n_\theta n_z)^2 + n_\theta n_z$, whereas the total number for the SNBC boundary condition is $7(n_r - 1)n_\theta n_z + n_\theta n_z(n_\theta + n_z) + n_\theta n_z$ which is considerably smaller. In Table II we present some results for $R = 2.0$ with $n_r = 80$, $n_\theta = 60$, $n_z = 21$; for comparison we have also included the results for the two local boundary conditions even though they do not give completely satisfactory results for $R = 2.0$. The total execution time for the first two methods is broken up into calculation of the matrix elements and the solution of the linear equation system; for the last two methods time required for the calculation of matrix elements is negligible. These particular calculations were carried out on a Pentium 90 workstation using the NAG Fortran 90 compilers. Similar results were obtained on an IBM R6000 350 workstation. It is clear that if a more sophisticated preconditioner were applied in the sparse matrix solver, smaller computation times would result.

It is interesting to note that we have decreased the number of nonzero elements by a factor of 4 when going from the DDtN boundary condition to the SNBC and this results in a decrease of a factor of 3 in execution time.

ACKNOWLEDGMENT

One of the authors (H.R.) received a research grant from NSERC.

REFERENCES

1. J. B. Keller and D. Givoli, *J. Comput. Phys.* **82,** 172 (1989).
2. G. J. Fix and S. P. Marin, *J. Comput. Phys.* **28,** 253 (1978).
3. A. Bayliss, M. Gunzburger, and E. Turkel, *SIAM J. Appl. Math.* **42,** 430 (1982).
4. B. Engquist and A. Majda, *Math. Comput.* **31,** 629 (1977).
5. R. C. MacCamy and S. P. Marin, *Int. J. Math. Math. Sci.* **3,** 311 (1980).
6. S. P. Marin, *IEEE Trans. Antennas Propag.* **AP-30,** 1045 (1982).
7. D. Givoli and J. B. Keller, *Comput. Meth. Appl. Mech. Eng.* **76,** 41 (1989).
8. A. S. Deakin and J. R. Dryden, *J. Comput. Appl. Math.* **58,** 1 (1995).
9. C. K. W. Tam and J. C. Webb, *J. Comput. Phys.* **113,** 122 (1994).
10. D. Givoli, *J. Comput. Phys.* **94,** 1 (1991).
11. R. Barrett *et al., Templates for the Solution of Linear Systems* (SIAM, Philadelphia, 1994).